Journal of *Marine Science and Engineering*

MDPI

*Article*

# The Construction Conditions of a Pre-Piling Template for Foundations of Offshore Structures

**Deokhee Won [1,*], Jihye Seo [2], Osoon Kwon [2], Hae-Young Park [2] and Hyoun Kang [2]**

[1] Department of Urban Infra Engineering, Halla University, Wonju-si 26404, Republic of Korea
[2] Korea Institute of Ocean Science and Technology, Busan 49111, Republic of Korea; jhseo@kiost.ac.kr (J.S.); osoon@kiost.ac.kr (O.K.); hypark@kiost.ac.kr (H.-Y.P.); hkang@kiost.ac.kr (H.K.)
* Correspondence: thekey.won@halla.ac.kr; Tel.: +82-33-760-1263

**Abstract:** The foundations of offshore wind power can be classified as floating, tripod, jacket, monopile, or gravity-based, depending on the support type. In the case of tripod- and jacket-type supports, the structures require precise construction. There are two main methods for installing substructures: post- and pre-piling. The post-piling method involves moving the completed substructure to the site and fixing it to the seabed by inserting a pile into the leg pile and driving it, allowing it to be constructed without special off-shore equipment; however, the construction period is long. Contrarily, the precision of foundation installation can be improved by installing a pre-piling template, which is special equipment that serves as a basic structure, on the seabed in advance, and subsequently inserting substructures. This study presents a new type of underwater pre-piling template and method for achieving optimal construction environment conditions. Construction precision was analyzed based on the wave condition, current speed, winch speed, wave direction, and current direction while the under-water template was anchored to the seabed. It was found that the wave conditions, winch speed, and vessel type had a significant influence. The results obtained considering the Douglas sea scale show that precise construction could only be achieved within Grade 2 for general barge ships, while jack-up barge ships could be used even at Grade 3 or higher. The higher the winch speed, the more stable construction becomes possible, and jack-up barges show greater constructability than general barges.

**Keywords:** offshore wind turbine; support system; pre-piling template; under construction



**Citation:** Won, D.; Seo, J.; Kwon, O.; Park, H.-Y.; Kang, H. The Construction Conditions of a Pre-Piling Template for Foundations of Offshore Structures. *J. Mar. Sci. Eng.* **2024**, *12*, 174. https://doi.org/10.3390/jmse12010174

Academic Editor: Puyang Zhang

Received: 8 December 2023
Revised: 4 January 2024
Accepted: 10 January 2024
Published: 16 January 2024



## 1. Introduction

As the demand for renewable energy increases, interest in offshore wind farms and construction has increased. Considering their economic feasibility, large-capacity wind power generators are being installed in deep-water areas far from the land. Installation technology and methodologies are important requirements for expanding market presence. Economic efficiency must be secured to maintain technological superiority. Recently, the offshore wind power industry and researchers have been investigating construction methods to improve construction quality [1].

Full-fledged plant construction for offshore wind power begins at ports and harbors, where generator parts are manufactured and transported. An offshore wind power system comprises a turbine, tower, and substructure. The general installation process for the system is as follows: First, the substructure is installed on the seabed, which supports the turbine. Once the substructure is installed, the vessel returns to the port to load the other parts. After installing the foundation by dividing it into several parts using a special ship, the wind tower is divided into two or three parts, transported by a barge, and assembled using a sea crane. After construction, the wind turbine is tested to ensure that it operates normally. After testing, electricity is produced and is ready to be sent to the grid.

A wind turbine comprises three parts: a rotor that converts wind energy into mechanical energy, a generator that converts mechanical energy into electrical energy, and a nacelle

and tower that accommodate the generator [2]. The foundation structures of offshore wind power can be floating, tripod, jacket, monopile, or gravity-based, depending on the type of support, as shown in Figure 1. The precise construction of the tripod- and jacket-type foundations is essential. This foundation can be fixed to the seabed to withstand the harsh natural external forces of towers and turbines, such as waves, tidal currents, and wind loads. Wu et al. assessed the allowable sea states for offshore wind turbine blade installation using time-domain numerical models and considered weather forecast uncertainty [3]. Aliyar et al. studied offshore crane loads during the installation of a wind turbine jacket substructure in regular waves [4]. Ciappi et al. studied integrated wave-to-wire modeling for the preliminary design of oscillating water column systems for installations [5]. Shaju and Joseph conducted a review of a wind turbine foundations. They investigated the soil structure interaction and loads effect of a floating system, hybrid foundations, and suction anchors [6]. Faraci et al. studied wave- and current-dominated combined orthogonal flows over fixed beds. This should be considered as it can cause erosion at the foundation of the wind turbine [7]. A simple model was proposed by Grant and Madsen to account for the effects of waves on currents. Otherwise, the hydrodynamic field investigated turned out to be quite simple and of not great interest [8]. Basack et al. studied the failure mechanism and design techniques of offshore wind turbine pile foundations. We refer to the damage mechanics of wind power support structures in this paper [9]. Lee et al. investigated the characteristics of an oscillating water column wave power converter installed in an offshore jacket foundation for a wind turbine system [10]. Also, Ha et al. proposed structural modeling and failure assessment of a spar-type substructure for five MW floating offshore wind turbines under extreme conditions in the east sea. The analysis mechanism of the floating structure is described in [11].

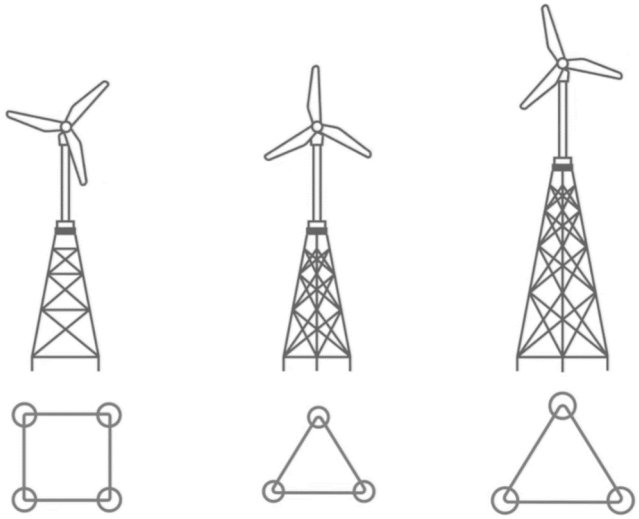

**Figure 1.** Foundation of wind power generation system.

If the support structures are not properly constructed on the seabed, adjusting the verticality, such as tilting the wind power generation system, can be difficult. There are two main methods for installing substructures according to the pile construction period: post-piling and pre-piling. The post-piling method uses a complete substructure. The piles are constructed via driving and excavation by inserting piles into the legs after mounting the substructure. This can be an efficient method without the need for special offshore equipment; however, the construction period is relatively long. Approximately 48 d are required to install one support structure.

Conversely, the pre-piling method was proposed to improve the accuracy of foundation installation. This method uses a template that serves as a foundation in advance. Piles are installed on the seabed, and substructures are inserted, mounted, and combined. The template is a configuration that guides pile construction. Piles can be installed while mov-

ing using a single template. This method has a faster overall construction speed than the post-piling method. However, the development of operational techniques for the template structure and consideration of the costs of the additional equipment are required. Generally, the pre-piling method is advantageous for constructing large-scale offshore wind farms of 300 MW or more.

Recently, various pre-piling templates have been developed and applied in this field. Improving the precision of the location is crucial when constructing newly developed templates. To accurately match the location on the seabed to that of the design, its hydrodynamic characteristics must be analyzed according to the ocean environmental conditions.

Most types of soil on the Korean seabed, which were the subjects of this study, are soft. For example, the coastal waters of Yeosu in the South Sea of Korea have soft ground that is approximately 30 m deep. If the template in Figure 2 is used, the template will penetrate the soft ground. In this study, small-scale suction anchors are installed on the template. This suction anchor prevents the template from penetrating into the soft ground.

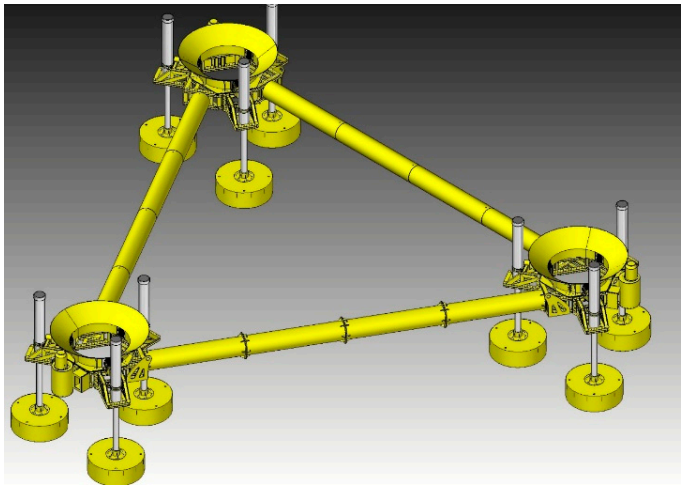

**Figure 2.** Conceptual design of triangular pre-piling template with suction anchors.

Thus, there are limitations to the application of a predeveloped template. Therefore, a new type of pre-piling template with a suction anchor is proposed, as shown in Figure 2. The triangular template components are detailed in Figure 3. The names of the parts shown in Figure 3a are as follows: ① is the bucket for fixing the foundation, ② is the leveling cylinder, ③ is the cylinder fixing module, ④ is the suction anchor, ⑤ is the hydraulic pressure sensor and its case, ⑥ is the base, and ⑦ is the centering cylinder module. This triangular template has three suction anchors attached to one main module, and the exact height can be adjusted using suction control. Further, according to the support structure type shown in Figure 1, the tripod can connect the three modules, as shown in Figure 3b. The jacket type can be configured by connecting the four modules to a template.

In this study, to achieve the optimal construction environment conditions for a triangular pre-piling template, the construction precision was analyzed based on the wave condition, current speed and direction, and winch speed, while the underwater template was anchored to the seabed.

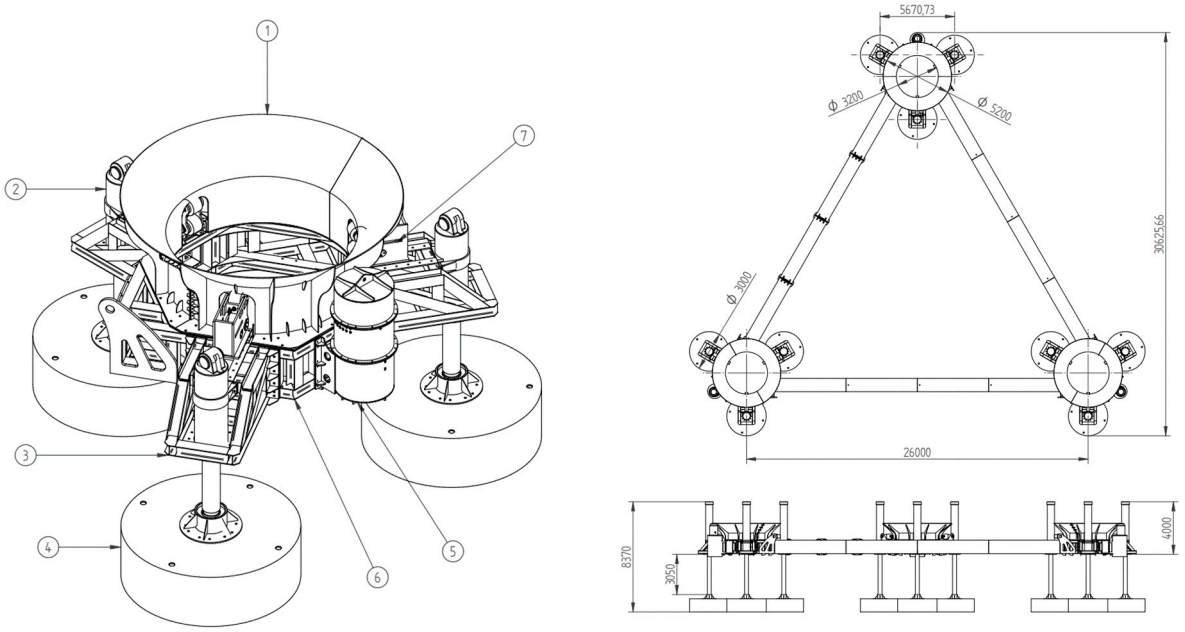


(**a**) entire view (**b**) plan view

**Figure 3.** Details of triangular pre-piling template with suction anchors (unit: mm).

## 2. Background

This study used Orcina 12 [12], a global statical and dynamic analysis tool for analyzing the environmental conditions during offshore construction. Objects such as buoys, cables, and ships can be subjected to finite element analysis using this analysis program.

### *2.1. Equations of Motion*

Equation (1) describes the motion in the time domain:

$$\boldsymbol{M}(\boldsymbol{p},\boldsymbol{a}) + \boldsymbol{C}(\boldsymbol{p},\boldsymbol{v}) + \boldsymbol{K}(\boldsymbol{p}) = \boldsymbol{F}(\boldsymbol{p},\boldsymbol{v},\boldsymbol{t}), \tag{1}$$

where $\boldsymbol{M}(\boldsymbol{p},\boldsymbol{a})$ is the inertial load of the system, $\boldsymbol{C}(\boldsymbol{p},\boldsymbol{v})$ is the damping load of the system, $\boldsymbol{K}(\boldsymbol{p})$ is the stiffness load of the system, $\boldsymbol{F}(\boldsymbol{p},\boldsymbol{v},\boldsymbol{t})$ is the external load, $\boldsymbol{p}$ is the position, $\boldsymbol{v}$ is the velocity, and $\boldsymbol{a}$ is the acceleration vector.

This program uses the extended Morison equation to analyze the hydrodynamic behavior of ships and buoys. This equation was proposed by Morison et al. (1950) [13] and can be written as

$$\mathbf{f} = \boldsymbol{C_m}\Delta\boldsymbol{a_f} + \frac{\mathbf{1}}{\mathbf{2}}\boldsymbol{\rho C_D A}|\boldsymbol{v_f}|\boldsymbol{v_f}, \tag{2}$$

where $\mathbf{f}$ is the fluid force per unit length of the body, $\boldsymbol{C_m}$ is the inertia coefficient of the body, $\Delta$ is the fluid mass displaced by the body, $\boldsymbol{a_f}$ is the fluid acceleration relative to Earth, $\boldsymbol{\rho}$ is the density of water, $\boldsymbol{C_D}$ is the drag coefficient of the body, $\boldsymbol{A}$ is the drag area, and $\boldsymbol{v_f}$ is the fluid velocity relative to Earth.

This equation can also be applied to systems that behave on a similar principle. In that case, the inertia term is reduced to $\boldsymbol{C_a}\Delta\boldsymbol{a_b}$, and the drag force term requires the body's relative velocity. In this analysis, the extended Morison equation was generated as follows:

$$\mathbf{f} = \left(\boldsymbol{C_m}\Delta\boldsymbol{a_f} - \boldsymbol{C_a}\Delta\boldsymbol{a_b}\right) + \frac{\mathbf{1}}{\mathbf{2}}\boldsymbol{\rho C_d A}|\boldsymbol{v_r}|\boldsymbol{v_r}, \tag{3}$$

where $\boldsymbol{C_a}$ is the added mass coefficient of the body, $\boldsymbol{a_b}$ is the body's acceleration relative to Earth, and $\boldsymbol{v_r}$ is the fluid velocity relative to the body.

### 2.2. Regular Waves

Equation (4) represents the Airy theory [13]. The expression u with time t and position (x, y) is expressed as follows:

$$\mathbf{u} = \mathbf{E}(\mathbf{z})\mathbf{a}\boldsymbol{\omega}\mathbf{cos}(\boldsymbol{\omega}\mathbf{t} - \boldsymbol{\varphi} - \mathbf{kx}), \tag{4}$$

where **a** is the wave amplitude, **ω** is the angular frequency, **φ** is the phase lag, **k** is the wave number, **x** is the horizontal position, z is the positive maximum value relative to the mean water level, and **E**(**z**) is a scaling factor in Airy's theory.

$$\boldsymbol{E}(z) = \frac{\boldsymbol{cosh}(\boldsymbol{k}(\boldsymbol{d}+\boldsymbol{z})}{\boldsymbol{sinh}(\boldsymbol{kd})} \tag{5}$$

In Equation (5), **d** denotes the mean water depth. This is an exponential decay term, in which the fluid velocity decreases with increasing depth.

### 2.3. Finite Element Model

In this study, a time-domain analysis was performed for hydrodynamic analysis, as shown in Figure 4. The time-domain analysis was completely non-linear. The mass, damping, stiffness, and load were evaluated at each time step. The time-domain principle was implicit. The dynamic behavior began based on the static analysis results. The time history data were obtained from the time-domain analysis. Moreover, the natural frequency analysis results were obtained from a static analysis [13].

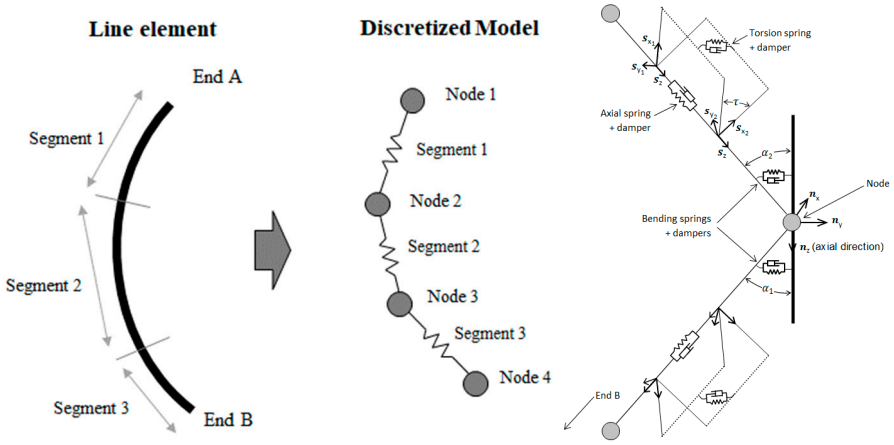


**Figure 4.** Principles of the line model (Orcina 12 [12]).

Orcina 12 [12] used FEM analysis. The beams, cables, and other parts were divided into several line elements. Only the axes and torsions were considered for the line elements. Buoyancy and weight were all calculated at the nodes. The segment consisted of two coaxial rods connected by an axial torsion spring damper. The bending of the line element was represented by a rotating spring damper at the node. Two bending stiffness values were specified for each element.

### 2.4. Joint North Sea Wave Project (JONSWAP) Spectrum

The Joint North Sea Wave Project (JONSWAP) [14] theory proposes an irregular wave spectrum based on measured data obtained through the JONSWAP project conducted in 1968–1969 in the North Sea. These waves can be applied to coastal wind waves. The power spectrum is created using Equation (6). Using the power spectrum, the amplitude

is determined by discretizing each period, and then, a random phase is generated from 0 degrees to 360 degrees to generate a wave propagation.

$$S(\omega) = \frac{\alpha}{c_1} = S_{PM}(c_1)\gamma^{exp[-(\omega-\omega_m)^2/2(\sigma\omega_m)^2]}, \quad (6)$$

In Equation (6), $\gamma$ is called the peak-shape parameter (3.3 on average) and represents the ratio of the maximum spectral energy density to the maximum of the Pierson–Moskowitz spectrum; $\alpha$ is a scale parameter $(0.076\bar{x}^{-0.22})$; $\sigma = 0.07, \omega < \omega_m$, $0.09\omega > \omega_m$; $\omega_m = 2\pi \times 3.5(\frac{g}{U})\bar{x}^{-0.33}$; $\bar{x} = \frac{gx}{U^2}$ is the dimensionless fetch; and $x$ is the fetch length (in m).

## 3. Verification of the Analysis Model Compared with Hydraulic Experiments

In this study, the marine environmental conditions during the construction of a pre-piling template were determined using hydrodynamic analysis. However, hydrodynamic experiments on pre-piled templates have not yet been performed. Because direct verification of the analysis method is impossible, the results of hydraulic experiments on underwater pipelines were used as Figure 6 [15]. The underwater pipeline experimental model has an elliptical cross section and is moored with a vertical tether. These cable elements and pipeline bodies are considered applicable because they are similar to the elements of the pre-piling template. The ORCINA 12 [12] used in this study completes the system using joint options and other boundary conditions for line and buoy elements when modeling the elements. Because these elements should be verified, they were compared and verified using the aforementioned repair experiments.

A two-dimensional wave flume was used as a hydraulic test device. It was 53 m long, 1.25 m high, and 1 m wide. The middle part of the hydraulic experiment was made of tempered glass to allow the experiment to be performed. A piston-type hydraulic pump was used to generate waves in the wave channel. The displacement was 50 cm. Wave dissipation devices were built at the front and rear of the hydraulic test flume.

The actual diameter of the submerged floating pipeline model was 23 m. For the pipe, the tension-leg method was applied to the mooring type. The experimental size was scaled down to 1/100, considering the size of the flume. The length, width, height, and draft of the pipeline were 0.98, 0.215, 0.140, and 0.8 m, respectively. The specimen was waterproofed to prevent water from entering. A 22 kg steel weight was installed inside to adjust the ratio of buoyancy to self-weight. The motion of the pipeline was measured using digital video. The wave period was 1.3 s, and the wave height was set in the range of 0.032–0.130 m, as summarized in Table 1.

Table 1 lists detailed specifications for the analytical model. The dimensions of the pipeline were the same as those of the hydraulic experimental model, as shown in Figure 5. Acrylic was used, and the wall thickness, elastic modulus, and mass density were 0.01 m, 3.4 GPa, and 1.45 kg/m$^3$, respectively. The drag coefficient and added mass of the pipe body and mooring line are the values proposed for DNV RP-C205 [16]. The diameter of the mooring line was 0.0025 m, and the interval between the mooring lines was 0.490 m. The main body and mooring line should be connected using a joint option as Figure 6. The interaction option was applied in this analysis program. This option allows for the adjustment of six degrees of freedom for rotation and displacement. The interaction option can be used to connect each member in the pre-piling template model. If necessary, they can be fully fixed and rotated in each direction.

A time-domain analysis was also performed. Figure 7 shows the dynamic behavior of the pipeline. Because regular waves were applied, it can be confirmed that nonlinear elements did not appear. Figure 7a shows the sway motion, and Figure 7b shows the heave motion. As the wave height increased, the sway motion gradually increased. In the case of the heave motion, the higher the wave height, the greater the force pressing the pipe, resulting in greater vertical displacement. A comparison of the analytical and experimental results is crucial. The regular wave experimental results fit well, with almost no errors in the analytical results. Figure 8 compares the results of the hydraulic experiment and analysis.

Figure 8a shows a comparison of the sway motion, and Figure 8b shows a comparison of the heave motion. As shown in Figure 8, the experimental and analytical results are in good agreement. The tendency was good, and the error in the value was significantly small. These results confirm that the elements, joint options, and wave generation methods applied in the analysis were reasonable. The options provided and assumed in this analysis program were applied to the pre-piling hydrodynamic behavior analysis.

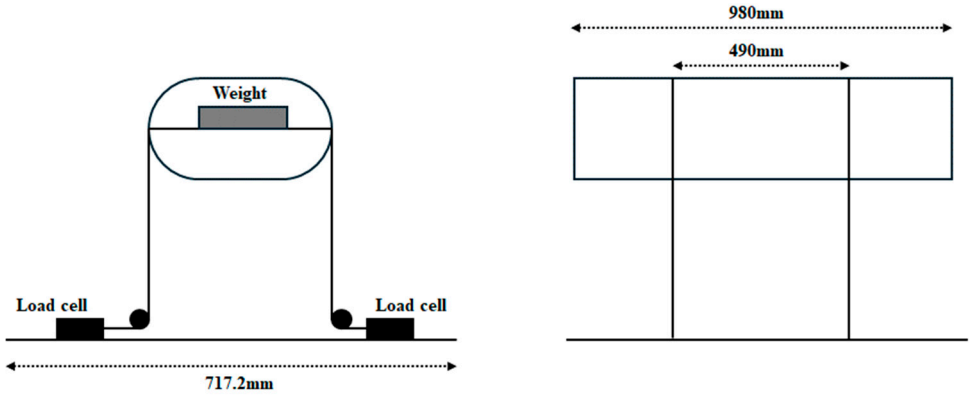


**Figure 5.** Setup of the hydraulic experiment [16].

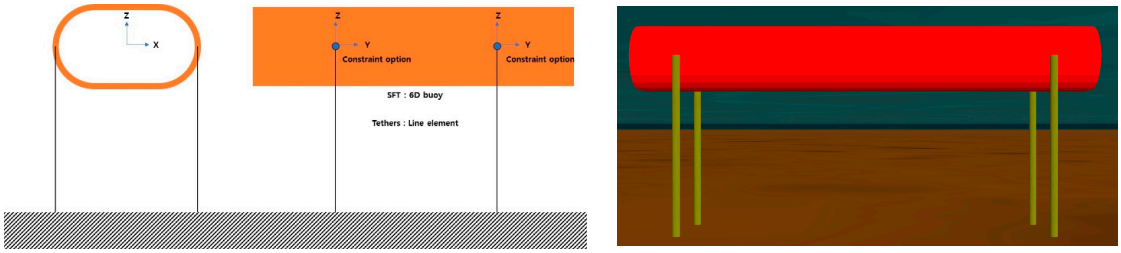


(**a**) (**b**)

**Figure 6.** Comparison between the hydraulic experiment and the analysis model. (**a**) Overview of the analysis model. (**b**) analysis model in Orcina 12 [12].

**Table 1.** Main properties and parameters of a small-scale pipeline.

| Parameters (Units) | Values |
|---|---|
| 1. Environmental conditions | |
| Water depth (h, m) | 0.8 |
| Wave period (T, s) | 1.3 |
| Wave height (H, m) | 0.032, 0.065, 0.098, 0.130 |
| 2. Pipeline | |
| Outer diameter (m) | 0.215/0.140 |
| Wall thickness (m) | 0.01 |
| Elastic modulus (GPa) | 3.4 |
| Density (kg/m$^3$) | 0.94 |
| Drag/added-mass coefficient (DNVGL-RP-C205 [17]) | 1.0/1.0 |
| Clearance depth (m) | 0.30 |
| 3. Tether | |
| Outer diameter (m) | 0.0025 |
| Elastic modulus (GPa) | 210.0 |
| Drag/added-mass coefficient (DNVGL-RP-C205 [17]) | 1.0/1.0 |
| Tether spacing (m) | 0.490 |

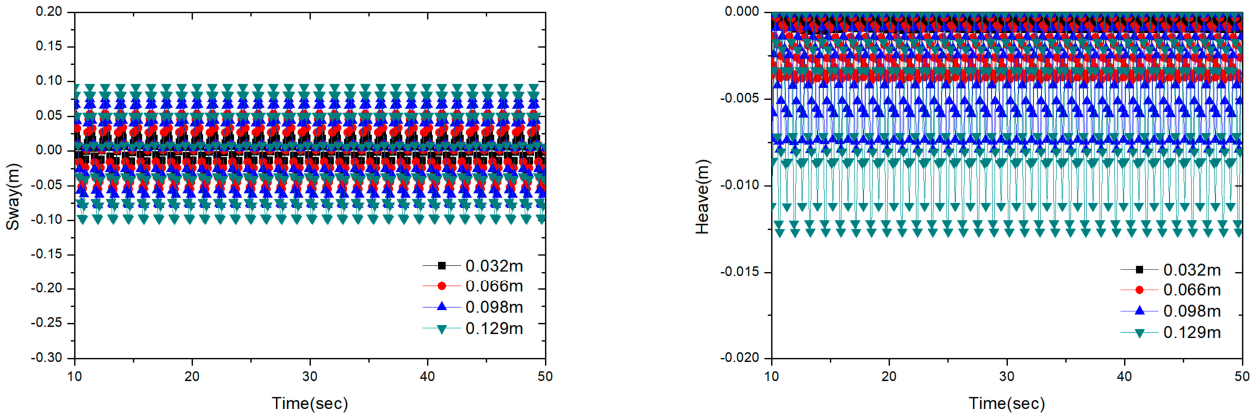


(**a**) sway motion (**b**) heave motion

**Figure 7.** Motion patterns in the SFT analysis model.

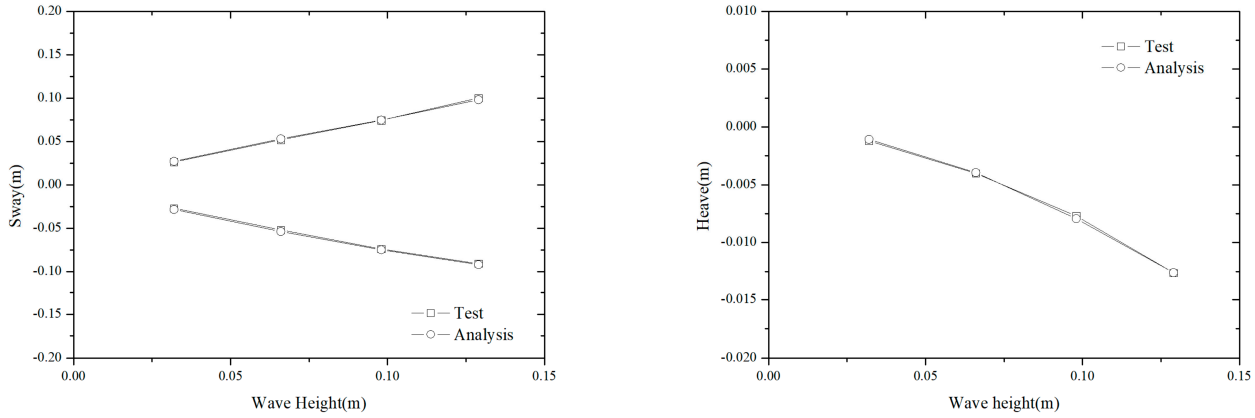


(**a**) sway motion (**b**) heave motion

**Figure 8.** Comparison of the experimental and analysis results.

Because hydraulic testing was not conducted on the target model, the analysis model was indirectly verified using the model in Figure 6. The components of the indirect comparison model consist of simple models such as body and cable. Additionally, the pre-piling template is simply composed of lifting cables, beams, and cylindrical columns, as shown in Figures 2 and 3. It is judged that there will be no difficulty in applying the boundary conditions, such as the member connection method, cross-section model, and environmental conditions, used in the above verification experiment model.

## 4. Hydrodynamic Behavior of Pre-Pilling Template under Different Ocean Environment Conditions

In this section, the proposed pre-piling template was modeled in Orcina 12 [12] using the analysis model verified in Section 2. After modeling each element, the behavioral characteristics were analyzed by applying waves and tidal currents.

### *4.1. Analysis Model*

Orcina 12 [12] provides basic simulation models such as ships, 6D buoys, line elements, and connecting options. In this study, the barge ship was assumed to have a width of 60 m and a length of 88 m, such that the suction anchor could be sufficiently loaded and unloaded. The ship shown in Figure 9 has the shape provided by the simulator. It was assumed that a crane and a winch were installed on the ship to lift the pre-piling template.

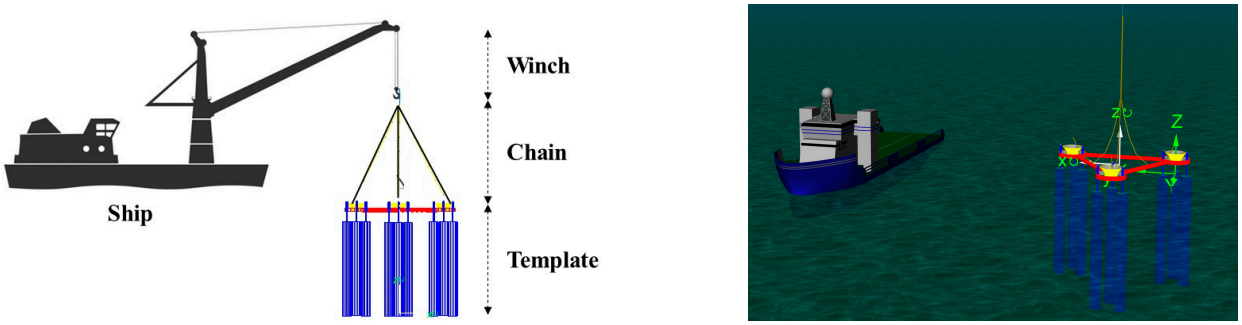


(**a**) lifting principal (**b**) analysis modeling

**Figure 9.** Analysis model based on Orcina [12].

Figures 9 and 10 illustrate the analysis model for the pre-piling template with a suction anchor based on Orcina 12 [12]. The various parts of the template mentioned in Figure 3 were simplified into modular models: bucket, base, and suction anchors. The bucket for fixing the foundation in Figure 10a had a cone shape with an upper outer diameter of 5.2 m, a lower outer diameter of 3.0 m, and a thickness of 0.1 m. The base part in Figure 10b is briefly expressed as a cylinder, and the total weight was set to 4.06 tf (4.06 × 9.81 KN). Figure 10c shows the suction anchor and pipe connecting to the base. The length of the suction anchor was 28 m, and the thickness of the connecting pipe was 0.01 m. They had a total weight of 20.81 tf (20.81 × 9.81 KN). The connecting pipe had an outer diameter, thickness, and weight of 1.06 m, 0.015 m, and 9.41 tf (9.41 × 9.81 KN), respectively, as summarized in Table 2. Three stud link chains were fixed to the winch installed on the barge ship to lift the pre-piling template. The stud-link chains had a diameter of 0.12 m and a length of 30 m.

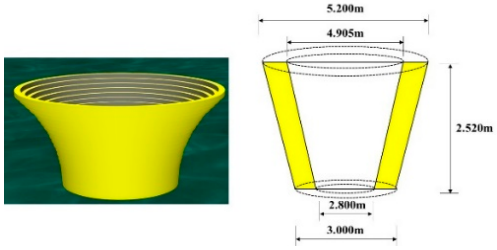


(**a**) bucket for fixing support legs

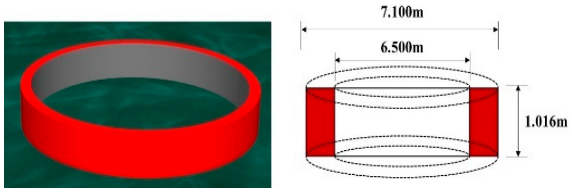


(**b**) base

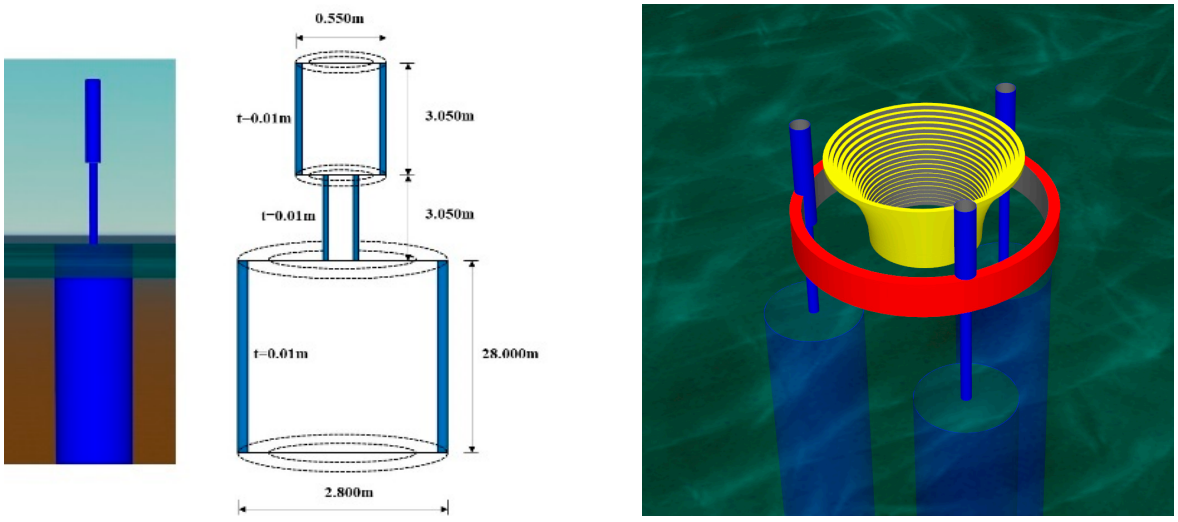


(**c**) suction anchor and leveling bars

**Figure 10.** Modular models of pre-pilling template.

**Table 2.** Mass properties of the modular models.

| Parts | Mass (kN/×9.81 KN) | Mass Moments of Inertia (kN.m$^2$) | | |
|---|---|---|---|---|
| | | x | y | z |
| Bucket | 34.85 | 87.0 | 87.0 | 137.0 |
| Base | 40.65 | 258.2 | 258.2 | 509.4 |
| Suction anchor | 208.1 | 16,470.4 | 16,470.4 | 373.9 |
| Connecting pipe | 94.1 | 2795.2 | 23.5 | 2795.2 |

The bucket, base, and suction anchors were modeled using a 6D buoy with a rigid body and six degrees of freedom: three translations (X, Y, and Z), and three rotations (rotations 1, 2, and 3). It was intended for use in the drag/inertia region where Morrison's equation was applied, and its diameter should be much smaller than the wavelength of the wave. These elements had both mass and moments of inertia and could model the forces and moments of various effects. A line connected to the 6D buoy model can be used to analyze both the instantaneous effect and transformation as the buoy rotates. A line was connected to an offset location in the buoy model.

### *4.2. Hydrodynamic Performance of Pre-Pilling Template*

Figure 11 shows the analysis conditions used to construct the pre-piling template on the seabed. A variable analysis was performed by considering the wave, current, and winch speeds. Fundamentally, irregular wave conditions were applied with an effective wave height of 1.25 m and an effective wave period of 4.5 s based on the JOHNSWAP spectrum. The speed of the tidal current was 2 m/s at sea level and became 0 m/s at the seabed as the depth decreased according to Equation (7) [16]. The winch speed was set to 0.5 m/s.

$$V_{c,tide}(z) = V_{c,tide}(0)\left(\frac{d+z}{d}\right)^{\alpha} for\ z \leq 0 \quad (7)$$

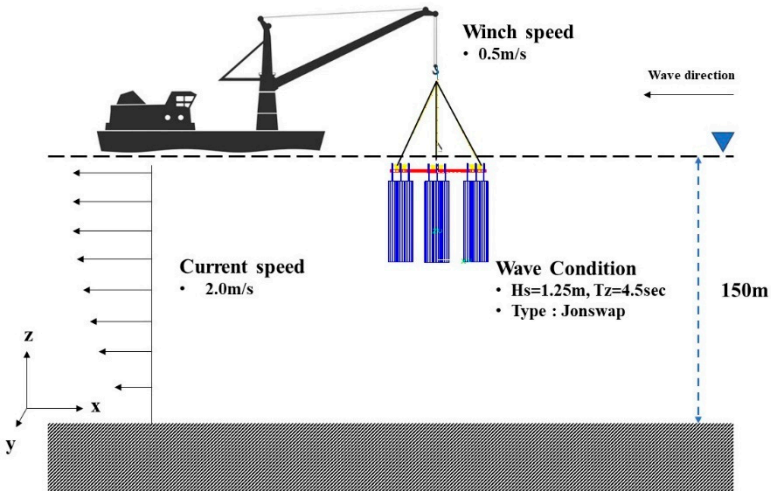


**Figure 11.** Analysis conditions ($H_s$: significant wave height, $T_z$: zero-up-crossing period).

Figure 12 shows the hydrodynamic behavior of the template. Figure 12a shows the irregular wave time series with the Johns pressure spectrum, and Figure 12b shows the von Mises stress of the lifting chain under wave loads, which generated a maximum of 110 MPa. As shown in Figure 12b–d, the stud link chain had a large amount of stress because the template motion was at its maximum at a depth of approximately 30 m from sea level. Waves had almost no effect at a depth of 60 m and above. It can be confirmed that the landing point on the seabed had a spacing of 5.85 m in the x-direction and 2.8 m in the y-direction from the target location. Figure 12c shows long-periodic oscillations. This

represents the natural vibration period of the cable, which is about 18 s when the cable is at its shortest, and increases to over 50 s as the length becomes longer. If the winch speed is 0.5 m/s, it should reach the bottom in 300 s. However, due to the influence of waves and current speed, it reaches the bottom in 450 s.

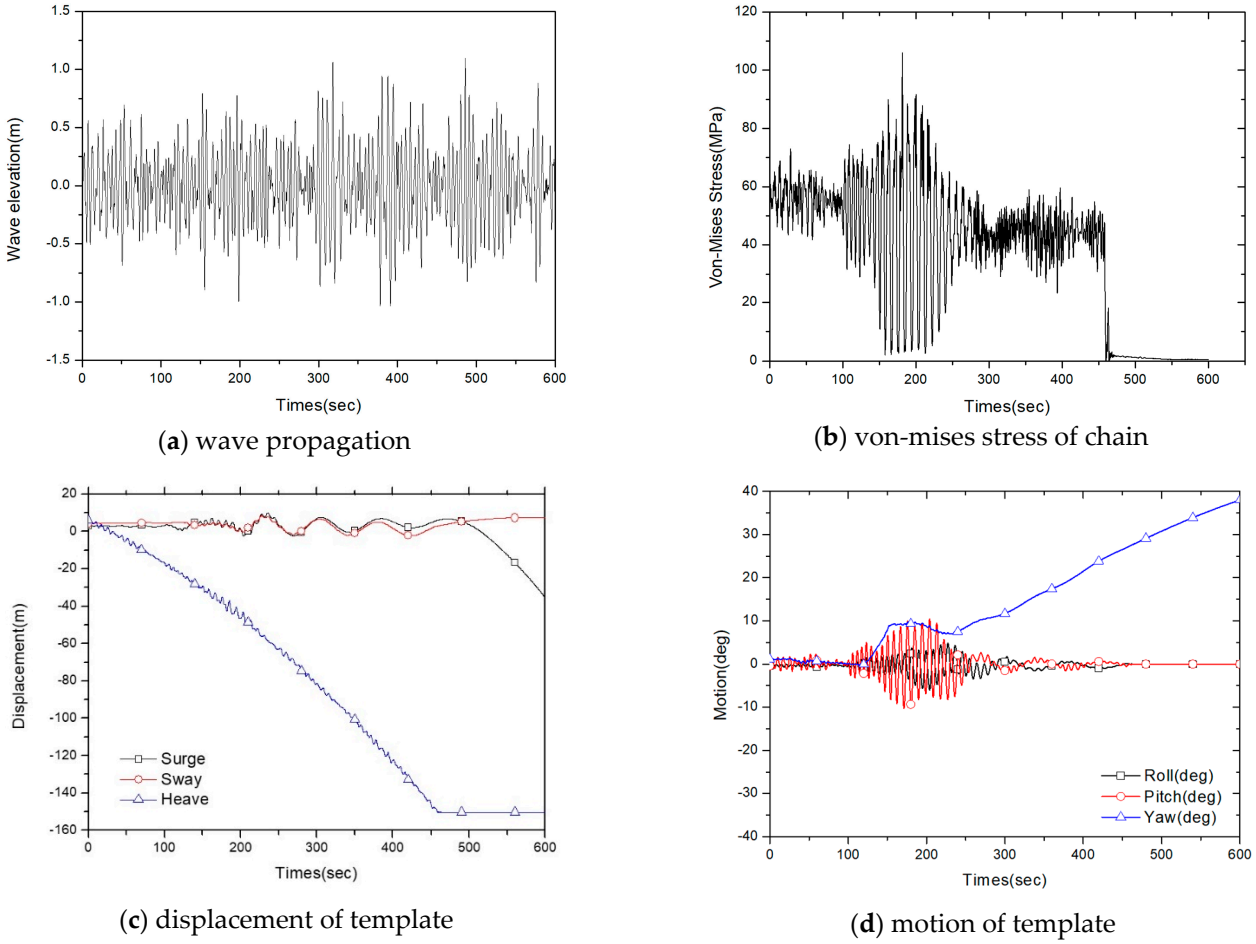


(**a**) wave propagation

(**b**) von-mises stress of chain

(**c**) displacement of template

(**d**) motion of template

**Figure 12.** Hydrodynamic behavior of template.

This analysis program does not consider penetration of the model into the ground. Therefore, it rotates because waves and currents continuously act on it, as shown Figure 12d.

## 5. Feasibility Study of Pre-Pilling Template under Different Ocean Environmental Conditions

In this section, the stress state of the chain and the motion of the template for the suggested pre-piling template under the mounting stage on the seabed were analyzed, assuming specific ocean environmental conditions and barge ship types. To install a template underwater, the mounting location must be determined. Therefore, behavior analysis of the pre-piling template, which can be associated with construction quality, under various ocean environmental conditions is crucial. In this study, this was analyzed by considering the height and period of the waves, speed and direction of the tidal current, and winch speed under various ocean environmental conditions. The ultimate permissible sea conditions for the underwater construction of the pre-piling template were examined.

### *5.1. Sea State Scale*

The Douglas sea scale [17] is an index used to measure wave heights and swells. This scale is expressed in 10 degrees from 0 to 9 based on the ocean environmental conditions proposed by the World Meteorological Organization (WMO). As it is an important index

for offshore work, ocean environmental conditions were selected based on this sea state. Table 3 lists the calculated wave periods corresponding to the largest wave heights for each scale in Table 4, using DNV C205 [16]. The wave period was distributed from 3.0 to 12.0 s. Here, the speed of the tidal current was set to 0 m/s and the winch speed to 0.5 m/s to analyze only the effect on wave conditions.

**Table 3.** Wave conditions.

| Sea State Scale | Height (m) | Period (s) |
|---|---|---|
| Grade 1 | 0.10 | 3.0 |
| Grade 2 | 0.50 | 4.0 |
| Grade 3 | 1.25 | 4.5 |
| Grade 4 | 2.50 | 7.0 |
| Grade 5 | 4.00 | 8.0 |
| Grade 6 | 6.00 | 8.5 |

**Table 4.** The Douglas sea scale (WMO).

| Sea State Scale | Height (m) | Description |
|---|---|---|
| Grade 0 | No wave | Calm (glassy) |
| Grade 1 | 0–0.10 | Calm (rippled) |
| Grade 2 | 0.10–0.50 | Smooth |
| Grade 3 | 0.50–1.25 | Slight |
| Grade 4 | 1.25–2.50 | Moderate |
| Grade 5 | 2.50–4.00 | Rough |
| Grade 6 | 4.00–6.00 | Very rough |
| Grade 7 | 6.00–9.00 | High |
| Grade 8 | 9.00–14.00 | Very high |
| Grade 9 | >14.00 | Phenomena |

Figure 13 shows the motion of the pre-piling template based on the Douglas sea scale. Scales 1 to 3 in Figure 13a–c were mounted on the seabed after 450 s without being significantly affected by waves. In the absence of considering tidal current speed, the pre-piling template exhibits nearly 10 m of displacement in surge and sway motion after descending to a depth of 60 m underwater, as shown in Figure 13c. As the cable becomes longer, the natural vibration period changes, and a long-period wavelength is generated accordingly. It vibrates according to the natural frequency at the time of lifting. According to the Douglas sea scale, the surge and sway motions increase as the wave and period increase. Unfortunately, for Grades 4 to 6 in Figure 13d–f, it can be observed that a large motion occurred, and underwater construction is deemed impossible.

The sea state is crucial during the construction process. High waves and long periods have a significant impact on the constructability of pre-piling templates. During underwater construction, we must precisely control the location of the ship. Therefore, the distance between the entry point and the landing position must be minimal. Otherwise, we will need to incorporate a positioning control system into the pre-piling system. As the sea scale rises, motion increases and constructability decreases accordingly.

The displacement results of the pre-piling template exhibited a similar tendency to those shown in Figure 13, as shown in Figure 14. The sway and surge motions represent the x- and y-directions, respectively. In Figure 14a, the Grade 2 sea state had a sway of 1.98 m and a surge of 0.97 m. Grade 3 increased the motions to 5.83 m for sway and 2.47 m for surge. However, in Figure 14b, assuming that a jack-up barge ship can fix the ship on the seabed, it was determined that the underwater work could be carried out with a displacement of 2 m less than that of Grade 3. This is because there was no ship motion other than that of a general barge ship. Thus, it can be concluded that the precision of underwater construction with the general barge ship was reduced by the affected wave loads.

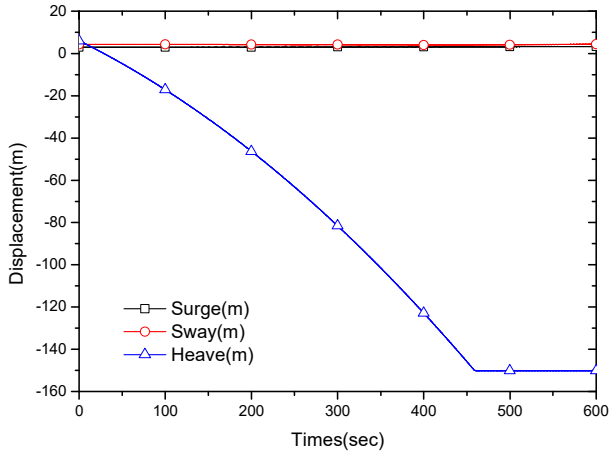


(**a**) Grade 1 of sea state

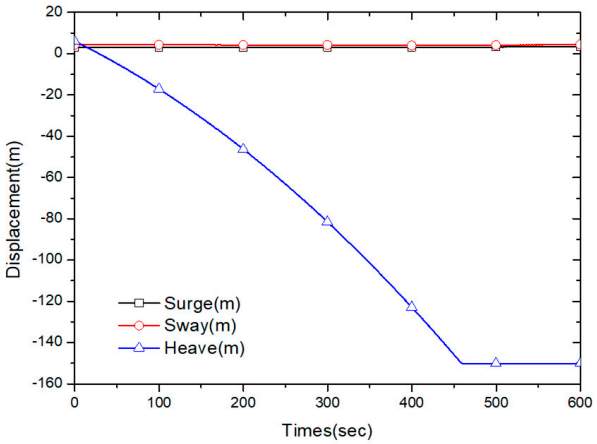


(**b**) Grade 2 of sea state

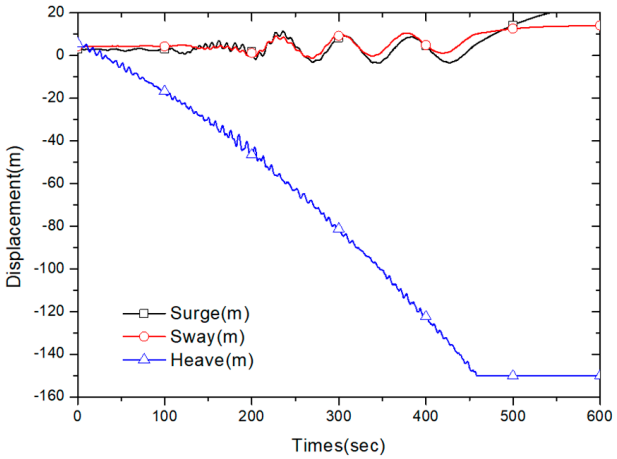


(**c**) Grade 3 of sea state

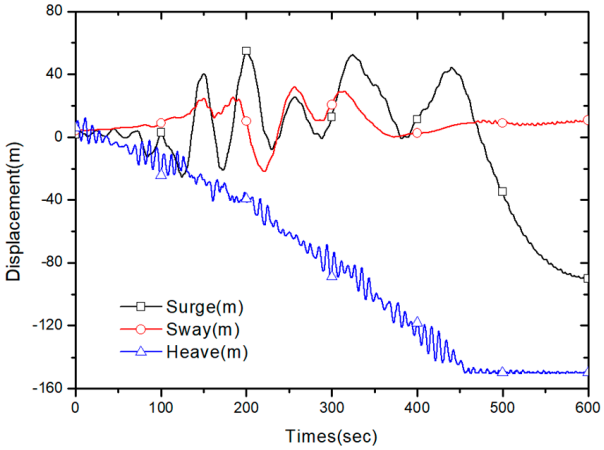


(**d**) Grade 4 of sea state

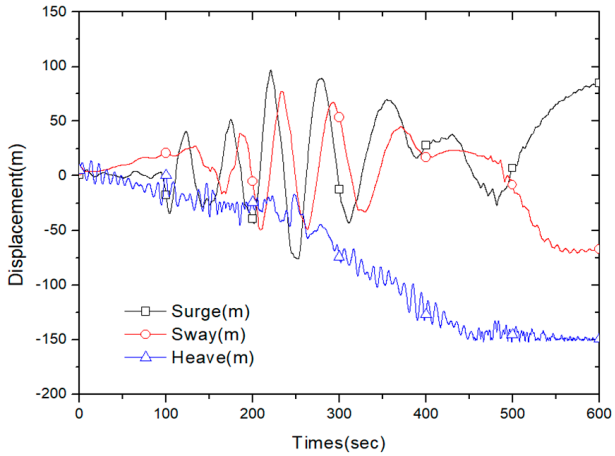


(**e**) Grade 5 of sea state

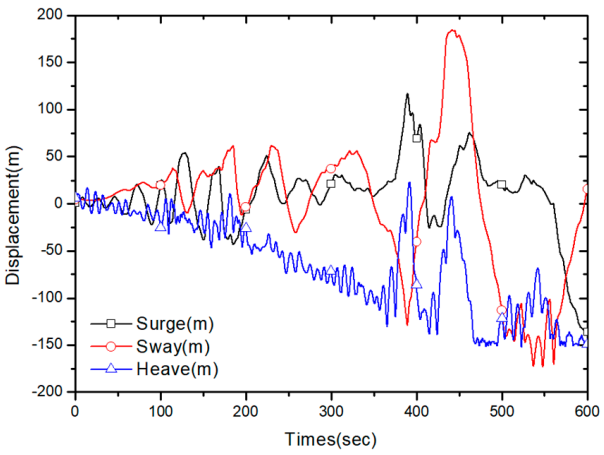


(**f**) Grade 6 of sea state

**Figure 13.** Motions of template by sea state.

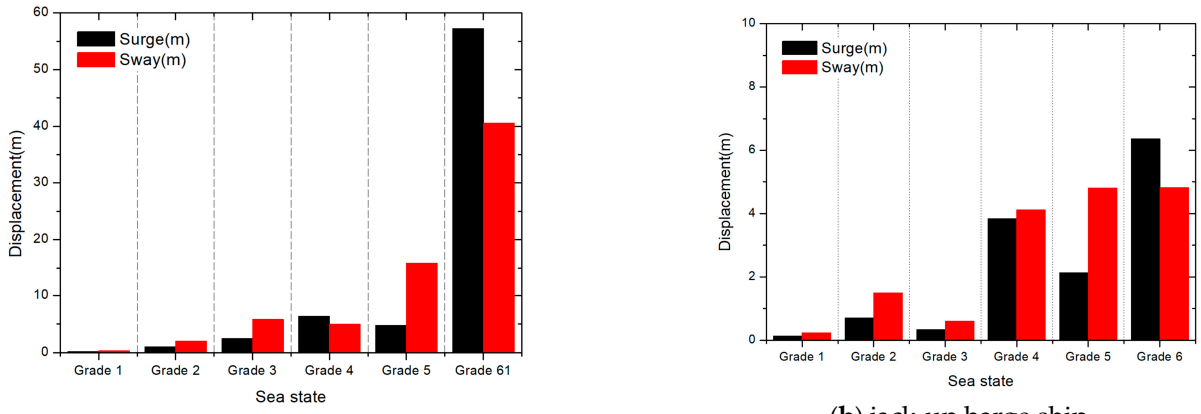


(**a**) general barge ship (**b**) jack-up barge ship

**Figure 14.** Displacement of template by sea state according to barge ship type.

### *5.2. Speed and Direction of the Tidal Current*

The tidal current speed and direction also affect the construction precision of underwater templates. The template motion was examined by increasing the current speed from 0 to 2.0 m/s. As shown in Figure 15, the surge and sway motions showed little difference based on the variables until 300 s, owing to the dominant influence of the wave loads. Slight displacement occurred after 300 s, when the influence of the waves decreased. After the template was mounted on the seabed, it was observed that motions occurred continuously owing to the tidal currents. There was no large deformation because pile penetration occurred owing to its weight.

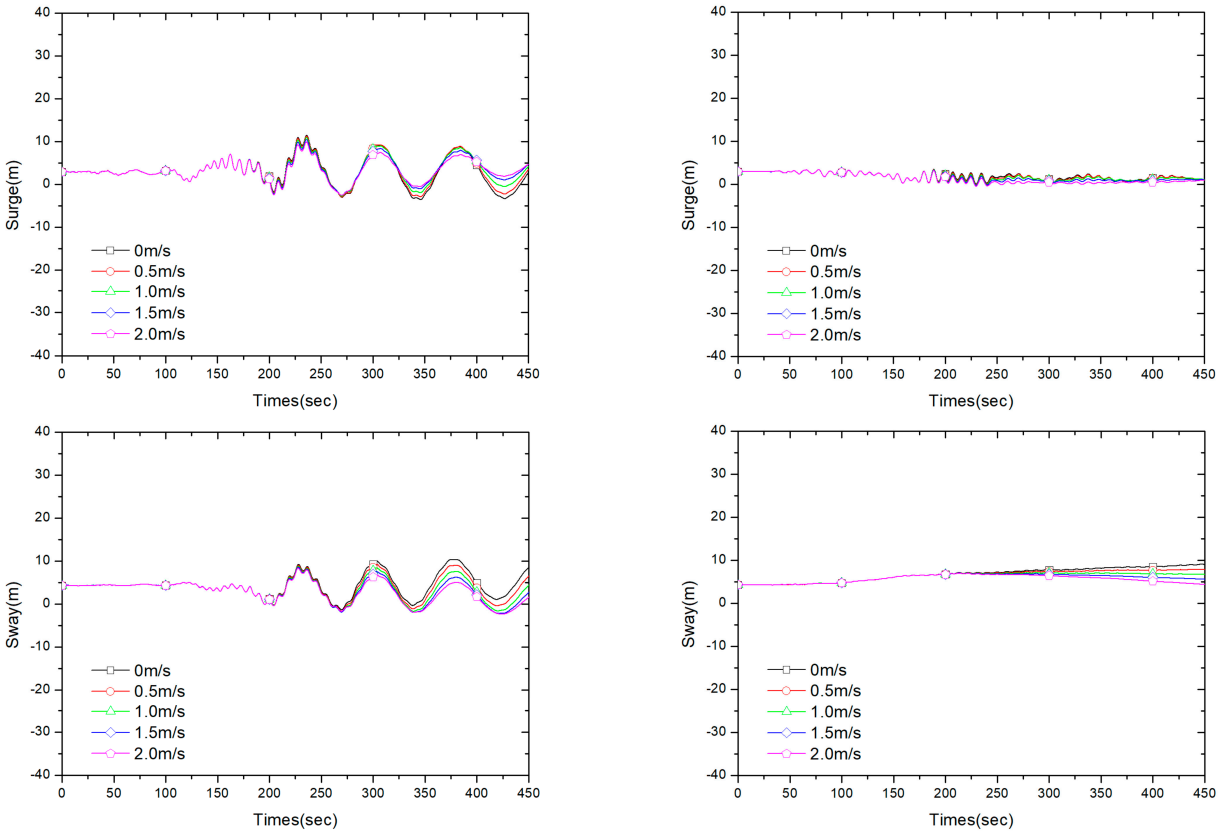


(**a**) general barge ship (**b**) jack-up barge ship

**Figure 15.** Displacement of template by current speed according to barge ship type.

The JONSWAP spectrum for irregular waves was applied to all models. Nevertheless, the surge and sway motions have almost identical periods, and differ only in amplitude. In subsea construction, the landing point is very important. If the landing point deviates significantly, it becomes difficult to set the exact location. As a result of the sway motion, there was a final difference of about 7 m between the positions at 0 m/s and 2 m/s. It was determined that as the depth of water increases, surge motion is greatly affected by current speed.

Figure 16 shows the rotations of the template under construction with tidal current speed, categorized by barge ship type. Here, the roll and pitch motions are represented by the angles of the $x$-axis and $y$-axis, respectively. When construction was performed on a general barge ship (Figure 16a), the rotations were larger than those of the jack-up barge ship (Figure 16b). Furthermore, as the current speed increased, the roll and pitch motions decreased from the water depth of 40 m, where the wave effect decreased. Changes in current speed have little effect on the pitch and roll motions before 200 s. However, after 200 s, the pitch and roll motions appear to decrease as the speed increases. As mentioned earlier, this is highly correlated with water depth. After 40 m of water depth, the amplitude of the roll and pitch motions decreases as the current speed increases.

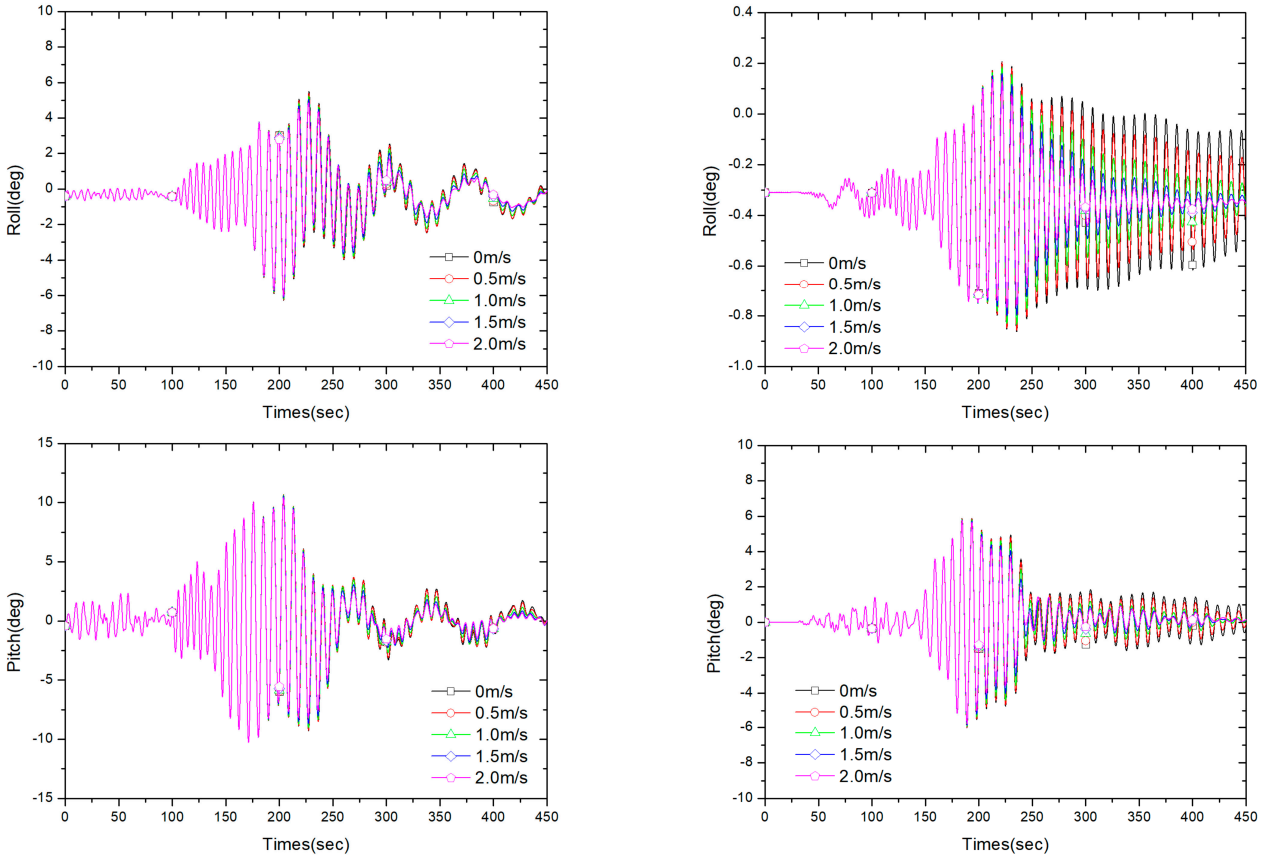


(**a**) general barge ship (**b**) jack-up barge ship

**Figure 16.** Template rotations by current speed according to barge ship type.

Figure 17 illustrates the influence based on the current direction. The largest sway occurs when the tidal current flows in the same direction as the wave and decreases when the current flows in the opposite direction to the wave. However, there is little difference in the case of roll and pitch motions. The surge, pitch, and roll motions exhibit almost identical behavioral characteristics regardless of the current direction. However, the sway motion gradually changes significantly after 200 s. The analysis reveals that the speed and

direction of the current do not significantly affect the winch speed in comparison to the wave height and period.

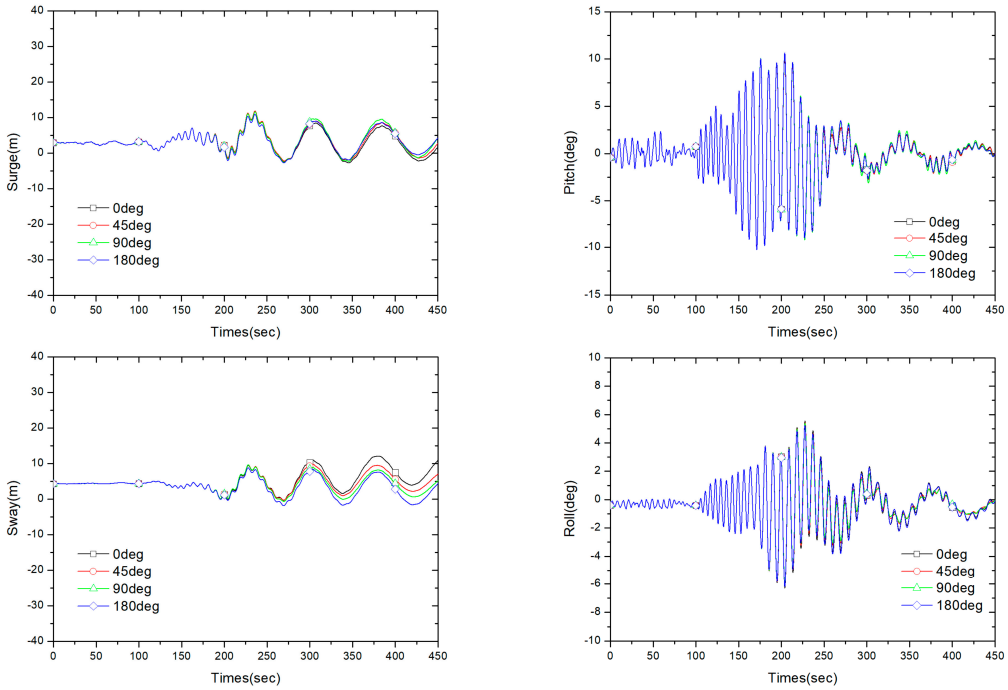


**Figure 17.** Template motions by current direction according to barge ship type.

### *5.3. Winch Speed*

Figures 18 and 19 show the template motions based on winch speed. The template motions were analyzed by changing the winch speed from 0.5 to 1.1 m/s in the Grade 3 sea state (1.25 m and 4.5 s), and the current speed was set to 1.0 m/s. Figure 18 shows the comparative results of the surge and sway motions in general and jack-up barge ships, where it can be observed that the motion was relatively small in jack-up barges. Generally, as the winch speed increased, the motion tended to decrease. This can also be observed in the roll and pitch motions, as shown in Figure 19. The smallest roll and pitch motions were observed at a winch speed of 1.1 m/s. Because the precision of constructability varies depending on the winch speed, it can be concluded that the winch speed should be controlled to suit specific sea conditions. Landing time varies depending on winch speed.

The sea bottom landing time is 315 s for 1.1 m/s, 350 s for 0.9 m/s, 390 s for 0.7 m/s, and 450 s for 0.5 m/s. As the winch speed increases, the model's motion decreases. The landing position is greatly affected by the positioning speed of general barges and jack-up barges. For general barges, if the winch speed is fast, there is no significant difference between the entering position and the landing position. In the case of a winch speed of 1.1 m/s, there is no significant surge or sway fluctuation. This means that a fast winch speed is good for general barges.

In contrast, the motion of a jack-up barge is different from that of a general barge. Comparing the sway motion, a winch speed of 1.1 m/s resulted in a difference of 4 m. 0.9 m/s resulted in a difference of 2 m, and 0.7 m/s resulted in a difference of 2.2 m.

The amplitude of pitch and roll motions decreases according to the winch speed increases for both ships. Overall, a higher winch speed reduces motion. However, for jack-up barges, it is important to find the optimal winch speed through preliminary simulation.

When comparing jack-up barge ships and regular ships, this has a significant impact on construction precision. In the case of jack-up barges, as the waves increase, barge motion and, after 200 s, long-term periodic motion of more than 10 m occur. However, jack-up

barge ships exhibit much smaller motions and do not generate long-period motions, leading to greater precision.

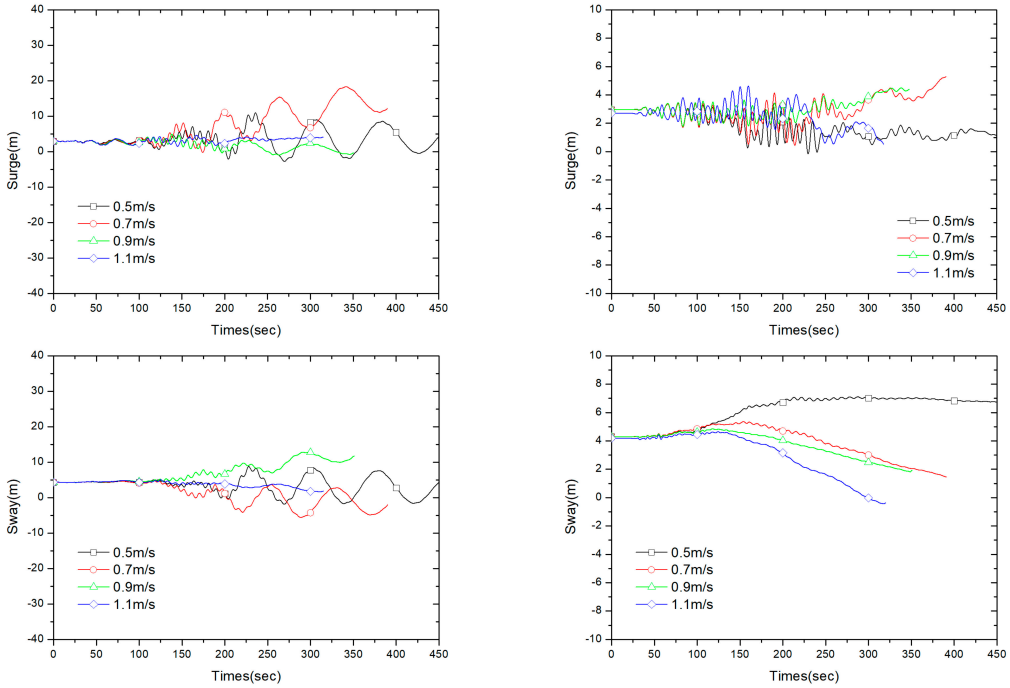


(**a**) general barge ship (**b**) jack-up barge ship

**Figure 18.** Displacement of template by winch speed according to barge ship type.

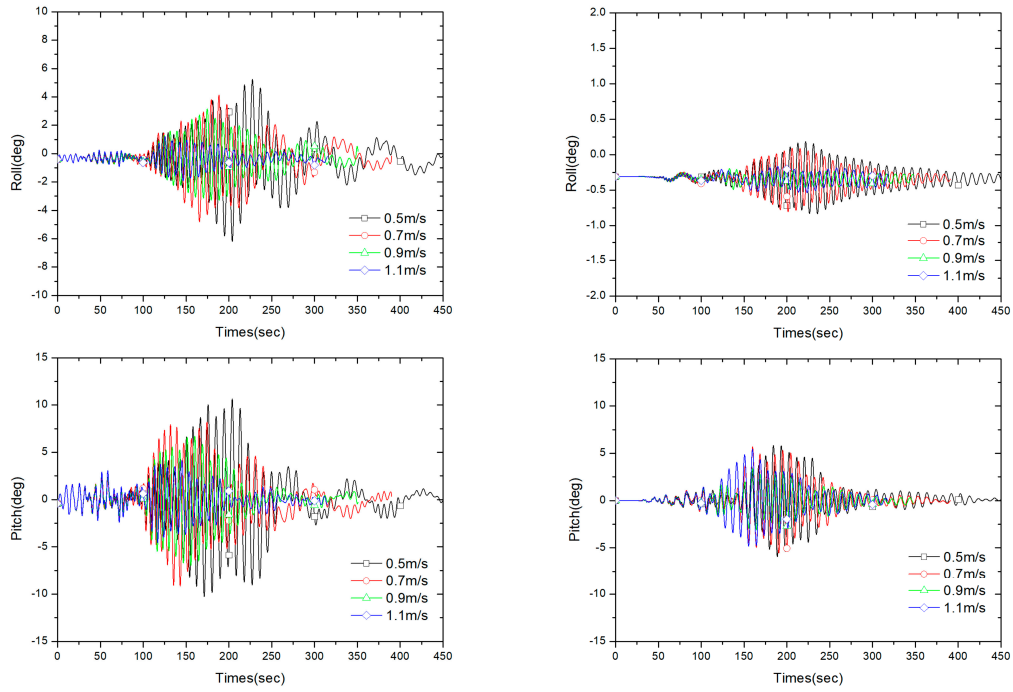


(**a**) general barge ship (**b**) jack-up barge ship

**Figure 19.** Template rotations by winch speed according to barge ship type.

## 6. Summary and Conclusions

In this study, the construction conditions of a new type of underwater pre-piling template under a mounting stage on the seabed were numerically analyzed, assuming

specific ocean environmental conditions and working ship types. The selected variables were the degree of sea state, speed, direction of the tidal current, and winch speed.

1. In the proposed pre-piling template, the length of the suction anchor varies depending on the depth of the soft ground. The maximum suction anchor length is 30 m. The hydrodynamic behavior of this model when exposed to the ocean environment was analyzed.
2. The pre-piling template reaches the seafloor in approximately 450 s when the winch speed is 0.5 m/s. The water depth is 150 m. At sea scale 1, long-period motion does not occur because the waves are small. However, at sea scale 3, long-period surge and sway motions last about 80 to 100 s, longer than the short-period motion caused by the wave period. This is due to the increase in the length of the winch cable, resulting in a natural frequency exceeding 80 s after 200 s.
3. Determining the economic aspects and selecting either jack-up or general barge ships are important considerations for underwater construction. Our results showed that the template motion decreased in all variable cases when the jack-up barge ship was used. This increased the positioning precision for underwater construction.
4. The results obtained considering the Douglas sea scale show that precise construction could only be achieved within Grade 2 for general barge ships, while jack-up barge ships could be used even at Grade 3 or higher.
5. According to the analysis results of the tidal current speed of approximately 2 m/s, the current speed began to have an effect at a water depth of 50 m or more, where the waves had a slight influence and the template motion decreased relatively as the current speed increased. Moreover, the template motion decreased when the direction of the tidal current was opposite to the direction of the wave.
6. For general barges, if the winch speed is fast, there is no significant difference between the entering position and the landing position. In the case of a winch speed of 1.1 m/s, there is no significant surge or sway fluctuation. This means that a fast winch speed is good for general barges. In contrast, the motion of a jack-up barge is different from that of a general barge. Comparing the sway motion, the winch speed of 1.1 m/s resulted in a difference of 4 m. A winch speed of 0.9 m/s resulted in a difference of 2 m, and of 0.7 m/s resulted in a difference of 2.2 m.
7. In wind power generation projects, the economic feasibility decreases when marine environmental conditions are poor. In the case of a ship, you must pay a ship usage fee even if you do not use it after renting it. Therefore, it is crucial to analyze the most optimal construction process. Therefore, cost-effective construction will be feasible if the process is planned by analyzing the winch speed and wave conditions that impact the construction process.

**Author Contributions:** Conceptualization: D.W. and J.S.; methodology: O.K.; software: H.K.; validation: D.W. and H.-Y.P. All authors have read and agreed to the published version of the manuscript.

**Funding:** This work was supported by the Korea Institute of Energy Technology Evaluation and Planning (KETEP) and the Ministry of Trade, Industry, and Energy (MOTIE) of the Republic of Korea (No. 20213030020110).

**Institutional Review Board Statement:** Not applicable.

**Informed Consent Statement:** Not applicable.

**Data Availability Statement:** Data are contained within the article.

**Conflicts of Interest:** The authors declare no conflicts of interest.

## References

1. Baert, B. Analysis of the Installation of a Series of Piles for Offshore Wind Turbine Foundations. Master's Thesis, University of Rostock, Rostock, Germany, 2014.

2. Thomsen, K.E. *Offshore Wind: A Comprehensive Guide to Successful Offshore Wind Farm Installation*, 2nd ed.; Elsevier: London, UK, 2012.
3. Wu, M.; Gao, Z.; Zhao, Y. Assessment of allowable sea states for offshore wind turbine blade installation using time-domain numerical models and considering weather forecast uncertainty. *Ocean Eng.* **2022**, *260*, 111801. [CrossRef]
4. Aliyar, S.; Meyer, J.; Sriram, V.; Hildebrant, A. Experimental investigation of offshore crane load during installation of a wind turbine jacket substructure in regular waves. *Ocean Eng.* **2021**, *241*, 109979. [CrossRef]
5. Ciappi, L.; Simonetti, I.; Bianchini, A.; Cappietti, L.; Manfrida, G. Application of integrated wave-to-wire modelling for the preliminary design of oscillating water column systems for installations in moderate wave climates. *Renew. Energy* **2022**, *194*, 232–248. [CrossRef]
6. Shaju, A.; Joseph, N. A Review on Offshore Wind Turbine Foundations. *Int. Res. J. Eng. Technol.* **2022**, *9*, 448–454.
7. Faraci, C.; Musumeci, R.E.; Marino, M.; Ruggeri, A.; Carlo, L.; Jensen, B.; Foti, E.; Barbaro, G.; Elsaßer, B. Wave-and current-dominated combined orthogonal flows over fixed rough beds. *Cont. Shelf Res.* **2021**, *220*, 104403. [CrossRef]
8. Grant, W.D.; Madsen, O.S. The continental-shelf bottom boundary layer. *Annu. Rev. Fluid Mech.* **1986**, *18*, 265–305. [CrossRef]
9. Basack, S.; Goswami, G.; Dai, Z.-H.; Baruah, P. Failure-Mechanism and Design Techniques of Offshore Wind Turbine Pile Foundation: Review and Research Directions. *Sustainability* **2022**, *14*, 12666. [CrossRef]
10. Lee, H.H.; Chen, G.-F.; Hsieh, H.-Y. Study on an Oscillating Water Column Wave Power Converter Installed in an Offshore Jacket Foundation for Wind-Turbine System Part I: Open Sea Wave Energy Converting Efficiency. *J. Mar. Sci. Eng.* **2021**, *9*, 133. [CrossRef]
11. Ha, K.; Kim, J.-B.; Yu, Y.; Seo, H.-S. Structural Modeling and Failure Assessment of Spar-Type Substructure for 5 MW Floating Offshore Wind Turbine under Extreme Conditions in the East Sea. *Energies* **2021**, *14*, 6571. [CrossRef]
12. Orcina. Orcaflex 12. 2023. Available online: https://www.orcina.com/orcaflex/ (accessed on 9 January 2024).
13. Morison, J.R.; O'Brien, M.D.; Johnson, J.W.; Schaaf, S.A. The force exerted by surface waves on piles. *J. Pet. Technol.* **1950**, *2*, 149–154. [CrossRef]
14. Hasselmann, K.; Cartwright, D.E.; Hasselman, D.E.; Olbers, D.J. *Measurements of Wind-Wave Growth and Swell Decay during the Joint North Sea Wave Project (JONSWAP)*; Deutches Hydrographisches Institut: Hamburg, Germany, 1973.
15. *Development of Core Techniques for the Practical Use of Submerged Floating Tunnels*; Korea Institute of Ocean Science and Technology (KIOST): Busan, Republic of Korea, 2016.
16. *DVGL-RP-C205: Environmental Conditions and Environmental Loads*; DNV: Bærum, Norway, 2019.
17. WMO. *Guide to Wave and Forecasting (WMO-No 702)*, 2nd ed.; World Meteorological Organization (WMO): Geneva, Switzerland, 2018.